Available online at www.sciencedirect.com

ScienceDirect

Energy Procedia 137 (2017) 282–290

Energy Procedia

www.elsevier.com/locate/procedia

14th Deep Sea Offshore Wind R&D Conference, EERA DeepWind'2017, 18-20 January 2017, Trondheim, Norway

A comparison of two fully coupled codes for integrated dynamic analysis of floating vertical axis wind turbines

Boy Koppenol[a], Zhengshun Cheng[b,c,*], Zhen Gao[c], Carlos Simão Ferreira[d], Torgeir Moan[c]

[a]*Ventolines BV, Duit 15, Emmeloord 8305BB, The Netherlands*
[b]*State Key Laboratory of Hydraulic Engineering Simulation and Safety, Tianjin University, Tianjin 300072, China*
[c]*Department of Marine Technology, AMOS and CeSOS, Norwegian University of Science and Technology (NTNU), Trondheim, Norway*
[d]*Faculty of Aerospace Engineering, Delft University of Technology (TU Delft), Delft, The Netherlands*

Abstract

This paper presents a comparison of two state-of-the-art codes that are capable of modelling floating vertical axis wind turbines (VAWTs) in fully coupled time-domain simulations, being the HAWC2 by DTU and the SIMO-RIFLEX-AC code by NTNU/MARINTEK. The comparative study focusses on the way aerodynamics, hydrodynamics and structural dynamics are treated for DeepWind's 5MW Darrieus rotor mounted on a modified OC3 spar platform. The relevant modelling differences are described, followed by an introduction to the spar VAWT concept and selected load cases. Isolation of the aerodynamic model is achieved using an equivalent rigid land-based VAWT in steady wind-only environments. The added complexity in SIMO-RIFLEX-AC's aerodynamic model has shown to increase aerodynamic torque at tip-speed ratios above 2.5. Differences in the hydrodynamic and structural models were brought forward through fully coupled analyses in turbulent wind and irregular wave climates. It is found that the simplified mooring system in HAWC2 introduces a 2P yaw response (1P in SIMO-RIFLEX-AC), stronger motion coupling in surge-heave and a largely reduced mooring line tension since the dynamics of mooring lines are not considered. Indications are given that a higher tower mode is excited by 4P aerodynamic loading; an effect that is significantly stronger in HAWC2.

Peer-review under responsibility of SINTEF Energi AS.

Keywords: floating vertical axis wind turbine; code-to-code comparison; fully coupled simulations

* Corresponding author. Tel.: +47-73596004; fax: +47-73595528.
E-mail address: zhengshun.cheng@ntnu.no

1876-6102
Peer-review under responsibility of SINTEF Energi AS.
10.1016/j.egypro.2017.10.352

1. Introduction

An ever-increasing demand for electricity pushes the wind energy industry to deep waters that favour floating concepts. Floating horizontal axis wind turbines (HAWTs) are facing the challenges of high cost of energy; as an alternative, floating vertical axis wind turbines (VAWTs) have the potential to reduce the cost of energy and are thus of great interest. The VAWT was popular in North-America during the 1970s and 1980s, in this period considerable efforts were made to develop the Darrieus rotor [1]. Now, interest in floating VAWTs emerges for its simple design, low center of gravity and independence to wind direction. Potential benefits are reduced installation and O&M costs, blade manufacturing through the cost-effective pultrusion technique and possibly increased power efficiency [2].

In contrast with the conventional HAWT, the vertical axis rotor has a three dimensional swept volume that extends in the streamwise direction as well, which makes that a blade crosses the incoming wind flow in both the upstream- and downstream rotor half. The supporting platform should provide sufficient buoyancy and stability, which leads to a large structure with significant contribution from hydrodynamics. The mooring system is for station keeping and acts as a relatively soft spring compared to structural stiffness. Whilst our understanding of hydrodynamics and structural dynamics is fairly developed, VAWT aerodynamics is complex and introduces challenges with respect to load prediction. The floating VAWT system is highly dynamic and requires a fully coupled aero-hydro-servo-elastic simulation tool for accurate analysis. Presently only several publicly available codes have this capability, amongst them are the HAWC2 by DTU [3] and the SIMO-RIFLEX-AC code by NTNU/MARINTEK [4] that both account for aerodynamics through the Actuator Cylinder (AC) flow theory [5].

The work in this paper consists of a code-to-code comparison between SIMO-RIFLEX-AC and HAWC2 and is split to three parts: (1) demonstrating the general impact of dynamic stall, (2) illustrating the effect of different implementations of the AC flow theory and (3) presenting code-to-code differences in the dynamic response of a spar VAWT modelled in unsteady environments.

2. Numerical simulation tools

2.1. Aerodynamics

The aerodynamic loads are calculated using the AC flow model originally developed by Madsen [5]. A set of stacked cylinders is used to build the swept volume of the VAWT rotor. For numerical implementation Madsen has suggested a modified linear solution to solve the 2D flow problem of the individual cylinders. The solution that is implemented in HAWC2 contains an additional correction factor k_a for the induced velocities, as proposed by Madsen et al. [6]. Cheng et al. [7] further developed the model such that it accounts for the tangential loading term, inclination of blade elements and an additional correction to the induced velocities at higher tip-speed ratios. These developments are implemented in the aerodynamic model of SIMO-RIFLEX-AC. Hence the two codes correct the induced velocity differently, as highlighted by Fig. 1.

Dynamic stall is a phenomenon that occurs when the flow separates from the surface of the blade. For a VAWT it is likely to occur at low tip-speed ratios where the angle of attack changes more rapidly. Research has shown that it is essential to include the effect of dynamic stall for a more accurate prediction of the aerodynamic loads [8]. Due to its significance and hence sensitivity, it is chosen to match SIMO-RIFLEX-AC's dynamic stall model with the Stig Øye dynamic stall model implemented in HAWC2.

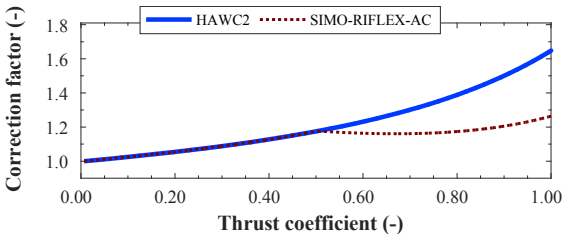

Fig. 1. Correction factor k_a in the modified linear solutions of the AC flow model.

Table 1. Hydrodynamic modelling in HAWC2 and SIMO-RIFLEX-AC. Morison coefficients are referred to [9].

	Spar hull		Mooring lines	
	HAWC2	SIMO-RIFLEX-AC	HAWC2	SIMO-RIFLEX-AC
Hydrodynamic model	Morison equation	Potential flow	none	Morison equation
C_d (-)	0.6	0.6	-	1.0
C_m (-)	0.97	Potential flow	-	1.0

2.2. Hydrodynamics

The hydrodynamic models in HAWC2 and SIMO-RIFLEX-AC are quite different in terms of complexity, an overview is given in Table 1. HAWC2 applies a Morison-type model for hydrodynamic loads on the spar. HAWC2 uses a non-linear spring model for mooring lines, hence no hydrodynamic loads and no inertial loads on the mooring lines are considered. SIMO-RIFLEX-AC applies a hybrid combination of the potential flow theory and Morison equation [10]. The potential flow model considers added mass, radiation damping, first order wave forces, mean drift forces and second-order difference-frequency wave forces on the spar floater. Mooring lines in SIMO-RIFLEX-AC are modelled as finite elements, where Morison's formula is used for hydrodynamic loads. The inertial effect of the mooring lines is considered in addition to the restoring effect.

2.3. Structural dynamics

The structural formulations in HAWC2 and SIMO-RIFLEX are both based on a finite element method with the spar platform modelled as one rigid body. HAWC2 applies a multi-body formulation with each body built from Timoshenko beam elements and connected by non-linear constraints, the mooring lines are simplified by a nonlinear spring model with an additional yaw stiffness to represent the delta lines. Riflex, the structural module in SIMO-RIFLEX-AC, distinguishes between the blades, tower (and shaft) and the mooring lines. These are respectively modelled as flexible beam elements, axisymmetric beam elements and nonlinear bar elements [10]. The delta lines within the mooring lines are also modelled by nonlinear bar elements.

3. Methodology

3.1. VAWT models

The dynamic analyses performed in this study involve the two wind turbine models in Fig. 2, referred to as the land-based VAWT and spar VAWT. The land-based VAWT considered is the 5MW Darrieus rotor developed by Vita [2] in the DeepWind project. The spar VAWT considers the same DeepWind rotor mounted on a ballast-modified OC3 spar floater [11].

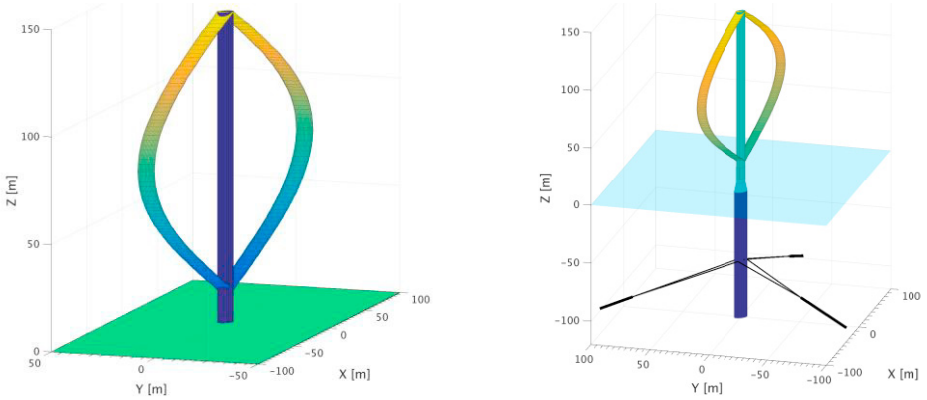

Fig. 2. The considered wind turbine models: (left) land-based VAWT; (right) spar VAWT.

Table 2. First six fundamental eigenmodes and eigenfrequencies of the land-based VAWT computed by Abaqus, HAWC2 and Riflex.

	Tower side-side 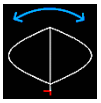	Tower fore-aft 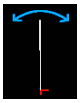	Flatwise symmetric 	Flatwise asymmetric 	Lead-lag asymmetric 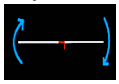	Lead-lag symmetric 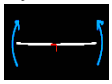
Abaqus [12]	0.207 *Hz*	0.223 *Hz*	0.270 *Hz*	0.272 *Hz*	0.342 *Hz*	0.421 *Hz*
HAWC2	0.205 *Hz*	0.222 *Hz*	0.277 *Hz*	0.278 *Hz*	0.372 *Hz*	0.475 *Hz*
Riflex [12]	0.204 *Hz*	0.220 *Hz*	0.268 *Hz*	0.269 *Hz*	0.352 *Hz*	0.428 *Hz*

For understanding the land-based VAWT characteristics a modal analysis is done in HAWC2, Riflex and Abaqus. This reveals information about the eigenmodes and eigenfrequencies, but also about the structural models of the numerical tools. Abaqus is considered most accurate and it can be used as benchmark for deviations between HAWC2 and Riflex. The six fundamental eigenmodes and corresponding eigenfrequencies are presented in Table 2. There can be distinguished between the tower, blade flatwise and blade lead-lag modes. In general, the eigenfrequencies between the codes agree well, except for the stiffer lead-lag modes where the structural formulation appears more critical. The modal analysis presented here considers a stationary rotor, hence the phenomena of centrifugal stiffening (flatwise) and gyroscopic effects (tower, lead-lag) are not included [12].

Where the land-based VAWT assumes a rigid connection to the ground, the spar VAWT is held in place by its catenary mooring system. The natural periods of the platform motions are obtained through decay tests and summarized in Table 3. The natural periods estimated by HAWC2 and SIMO-RIFLEX-AC are fairly close and the difference with respect to heave motion is due to the different modeling of mooring lines. The corresponding damping ratio in terms of surge and pitch motions are close too; however, large differences are observed in that of heave and yaw, which are owning to the different mooring line modeling in these two numerical codes.

Table 3. Natural periods and damping ratios of spar VAWT computed by SIMO-RIFLEX-AC and HAWC2.

	Natural period				Damping ratio			
	Surge (*s*)	Heave (*s*)	Pitch (*s*)	Yaw (*s*)	Surge (-)	Heave (-)	Pitch (-)	Yaw (-)
SIMO-RIFLEX-AC	129.0	27.0	34.6	7.4	0.078	0.046	0.037	0.094
HAWC2	129.4	32.0	34.5	7.6	0.077	0.092	0.047	0.049

3.2. Load cases

The offshore site that is considered in this study is located in the northern North Sea, a potential candidate for floating wind turbines off the Norwegian coast due to its large water depths. Johanessen et al. [13] correlated the wind-wave environment (wind speed, significant wave height and peak period) in this area using measurements taken at Statoil's oil platform Vestlefrikk.

The code-to-code comparison is performed for a set of pre-defined environmental conditions. The challenge in designing a set of test configurations is isolating the different models. The three load cases are detailed hereafter and summarized in Table 4. In all load cases wind shear is modelled as normal wind profile (NWP) and the controller keeps rotor speed approximately constant above rated wind speed of 14 *m/s*. The directions of wind and waves are collinear and along the spar's surge direction. Simulations with multiple seeds are grouped for statistical and spectral analyses.

Load case 1 (LC1) uses a rigid land-based VAWT to illustrate the effect dynamic stall over a range of wind speeds. For this purpose, LC1 is simulated in HAWC2 with and without the Stig Øye dynamic stall model.

Table 4. Load cases LC1, LC2 and LC3 for the code-to-code comparison between HAWC2 and SIMO-RIFLEX-AC.

	u_{hub} (*m/s*)	H_s (*m*)	T_p (*s*)	Turb. model	Seeds	Sim. length	Dynamic stall	VAWT configuration
LC1.1 / LC1.2	10 – 22	-	-	-	-	1600 *s*	None / Stig Øye	Land-based, rigid
LC2.1 / LC2.2 / LC2.3	8 / 14 / 20	-	-	-	-	4000 *s*	None	Land-based, rigid
LC3.1	8	2.55	9.86	NTM	3	4000 *s*	Stig Øye	Spar, elastic
LC3.2	14	3.62	10.29	NTM	3	4000 *s*	Stig Øye	Spar, elastic
LC3.3	20	4.87	10.86	NTM	3	4000 *s*	Stig Øye	Spar, elastic

Load case 2 (LC2) simulates the land-based VAWT in a steady wind environment. The structural elasticity is stiff and dynamic stall is not considered. These steps are taken to isolate the aerodynamic model in HAWC2 and SIMO-RIFLEX-AC to the extent that is possible. Three different wind speeds are considered, which allows us to compare the functionality of the aerodynamic models at a high, moderate and low tip-speed ratio.

Load case 3 (LC3) compares the fully coupled aero-hydro-servo-elastic capabilities of HAWC2 and SIMO-RIFLEX-AC. This is done by simulating the spar VAWT in a mild, medium and severe unsteady environment. Here dynamic analyses can be done only in terms of statistics and power spectra, because the stochasticity in the turbulent wind and irregular waves cannot be matched throughout the codes. The (statistical) agreement between the environmental conditions has been verified, and a seed sensitivity study showed that the order of differences also occur between the individual seeds.

4. Results and discussion

4.1. Effect of dynamic stall (LC1)

Simulating the land-based VAWT in a stepped wind environment allows us to study the effect of dynamic stall at various tip-speed ratios. The Stig Øye model disregards the effect on airfoil drag and hence only the lift component is affected, which Fig. 3 presents for the mid-point of blade 1. The loops present different tip-speed ratios at which the VAWT operates, with a decreasing tip-speed ratio for increasing angle of attack range. Data points off the 'lines' reflect the transient response after each wind step. The dynamic stall effect on the lift coefficient is strongest at larger angles of attack, and becomes significant below tip-speed ratios of approximately 2.5 for this configuration. The lift coefficient directly affects the calculation of lift force per unit length on the blade elements. In the upwind rotor half (positive angle of attack) lift force is much reduced from the effect of flow separation at lower tip-speed ratios. Consequently, the downwind rotor half experiences a higher inflow velocity and therefore increased lift.

To illustrate the difference with HAWT aerodynamics the rate of change in angle of attack can be observed. At the wind speed of 22 *m/s* (outer loop) the angle of attack at mid-blade changes from -35° to +40° in half a rotational period or 5.7 *s*, whereas the change is 0° for a HAWT in a uniform wind field.

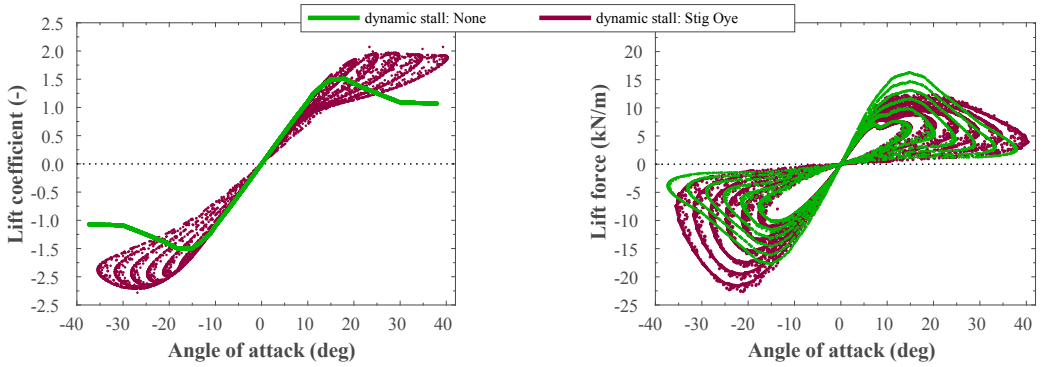

Fig. 3. Lift coefficient (left) and lift force (right) at midblade with tip-speed ratio decreasing stepwise from 3.5 to 1.5 in HAWC2 at LC1.

Table 5. Average thrust- and power coefficient for the land-based VAWT at LC2 in HAWC2 and SIMO-RIFLEX-AC.

	C_T (-)		C_p (-)	
	HAWC2	SIMO-RIFLEX-AC	HAWC2	SIMO-RIFLEX-AC
LC2.1	0.661	0.765	0.389	0.465
LC2.2	0.456	0.457	0.319	0.324
LC2.3	0.245	0.245	0.124	0.126

4.2. Comparison of aerodynamic model (LC2)

The aerodynamic model in HAWC2 and SIMO-RIFLEX-AC is isolated by placing the land-based VAWT in a steady wind field, this narrows the system down to an equilibrium between aerodynamic loads, rotor inertia and generator torque. At the low wind speed of LC2.1 the Darrieus rotor is in a region where C_p is optimized through a generator torque algorithm, whereas rotor speed is constant at the medium and high wind speed.

The rotor-averaged performance coefficients C_T and C_p of the VAWT at LC2 are presented in Table 5. Fig. 1 addressed that induced velocities are corrected differently between the codes for $C_T \geq 0.50$. Table 5 shows that this condition is reached only at LC2.1 for both codes. If dynamic stall effects were considered, then increased aerodynamic loads could potentially subject the induced velocities at LC2.2 to a different correction factor k_a as well.

To further explain the different performance, the aerodynamic torque is presented in Fig. 4. The time series at LC2.1 reveal that the torque has lower minima and higher maxima in SIMO-RIFLEX-AC. Torque minima occur when the VAWT rotor is perpendicular to the wind direction. The reduced torque can be related to inclusion of tangential terms in SIMO-RIFLEX-AC's aerodynamic model, because at this azimuth position the tangential terms are drag forces. The difference in aerodynamic torque maxima are however, a result of the correction factor k_a. HAWC2's larger correction factor at LC2.1 leads to lower inflow velocities in the downwind half of the rotor.

4.3. Comparison of fully coupled capabilities (LC3)

Dynamic analysis is done for the spar VAWT in unsteady wind-wave environments to compare the response in HAWC2 and SIMO-RIFLEX-AC. Platform motions are excited by aerodynamic and hydrodynamic loads, whereas the resulting offsets are counteracted by a restoring force from the mooring system and hydrostatic pressure differences. The platform response is described through statistical and spectral analysis in Fig. 5. Mean offset and standard deviation of all platform motions are lower in SIMO-RIFLEX-AC, also for the degrees of freedom not presented here. The heave response indicates motion coupling with surge in both codes, but stronger in HAWC2 due to a shifted natural frequency. The pitch response is stronger in HAWC2, which could be a result from applying

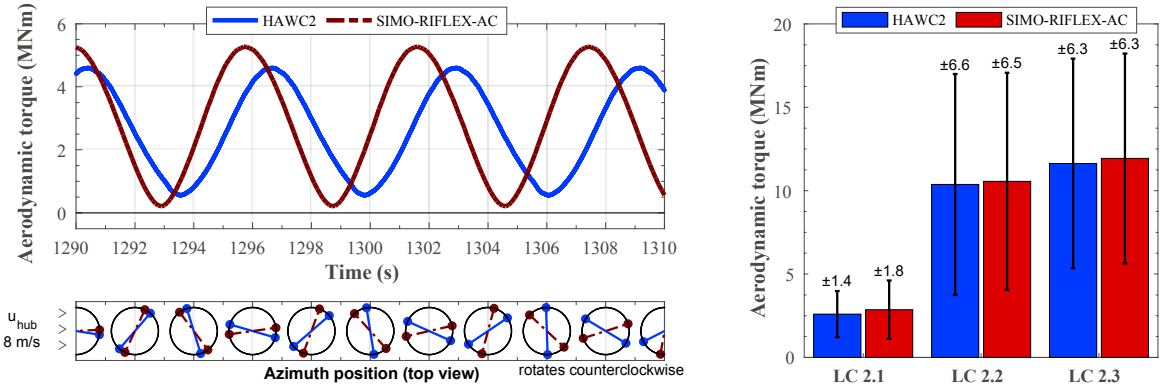

Fig. 4. Aerodynamic torque for the land-based VAWT: (left) time series at LC2.1; (right) mean and one standard deviation at LC2.

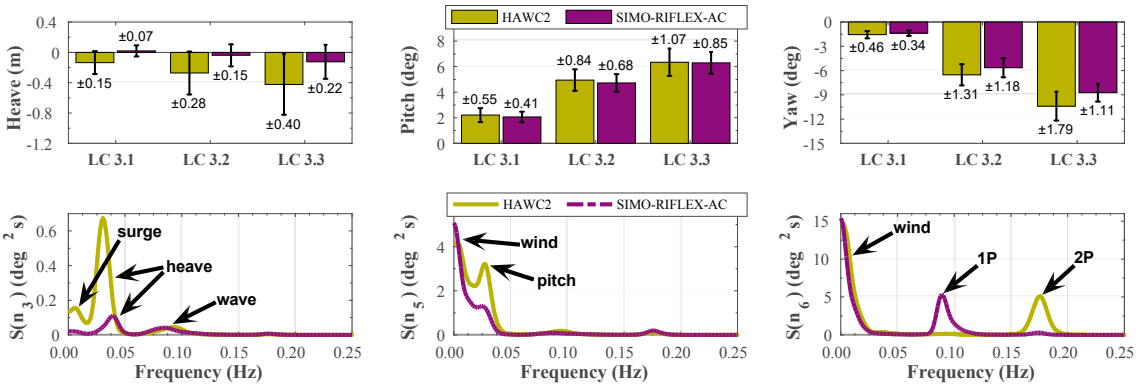

Fig. 5. Platform motions: (top) mean value and one standard deviation at LC3; (bottom) power spectral densities at LC3.2.

Morison equation on the spar hull. At last, the yaw responds at the 1P and 2P frequency in SIMO-RIFLEX-AC and HAWC2, respectively. The yaw natural frequency may have shifted due to different mooring system modelling, similar as to heave.

The mooring system provides stiffness for station keeping and loads are transferred through mooring line tension. A time series and statistical analysis of this tension in line 1 (see Fig. 2 for definition) is presented in Fig. 6. The time series reveal that the response is governed by low-frequent surge motion, however, SIMO-RIFLEX-AC also shows a vibration-like 1P response from its platform yaw. The tension in line 1 is lower in HAWC2 for all load cases and could reflect the absence of gravity-induced loads. Additionally, the absence of hydrodynamic loads on HAWC2's mooring system may also contribute to the lower standard deviations.

To get insight in the frequency content of aerodynamic loads from turbulent wind, spectral analysis of aerodynamic torque is presented in Fig. 7 (left). Characteristic for the two-bladed VAWT is that aerodynamics are governed by 2P loads, however, the codes reveal their differences at other frequency-content. SIMO-RIFLEX-AC finds additional contribution at the 1P and 3P frequencies, this could relate to its 1P yaw response. Both codes contain peaks at the 4P frequency, which seems to excite the first asymmetric lead-lag mode.

The structural models are compared through fore-aft bending moment at the tower base. The power spectrum in Fig. 7 (right) shows interesting differences with respect to platform pitch, wave loads and a structural mode. Here larger pitch offset – or tower tilt – leads to larger contributions from gravity. HAWC2's tower base feels the waves more strongly, which indicates that its hydrodynamic model calculates higher wave loading than SIMO-RIFLEX-AC's potential flow model. Dominant 2P responses are found in the power spectra of fore-aft bending moment

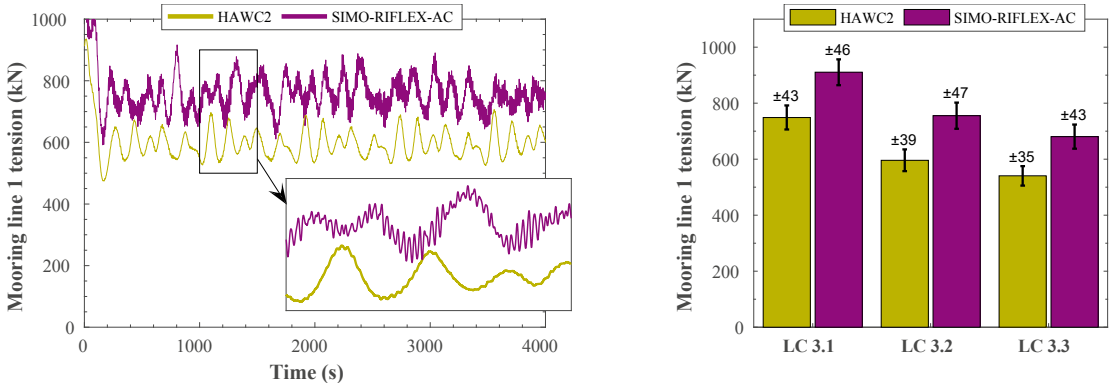

Fig. 6. Tension in mooring line 1: (left) time series at LC3.2; (right) mean and one standard deviation at LC3.

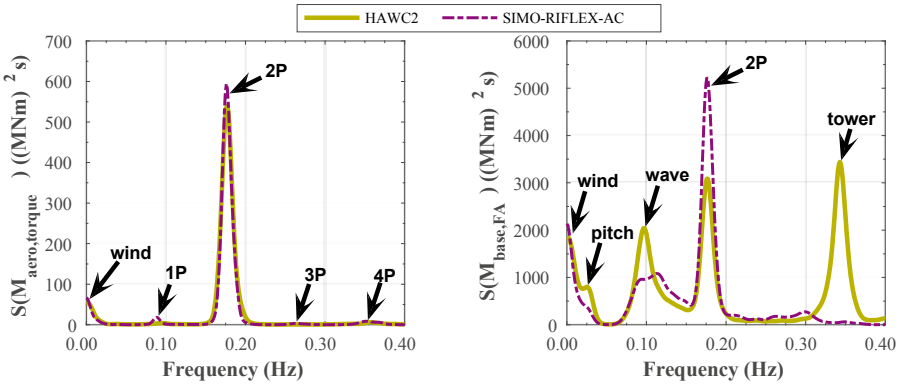

Fig. 7. Power spectral densities of aerodynamic torque (left) and fore-aft tower base bending moment (right) at LC3.2.

estimated by HAWC2 and SIMO-RIFLEX-AC, which are due to 2P aerodynamic loads on the blades. At last, a significant peak is found at 0.34 *Hz* only in HAWC2's spectrum. This hints towards a higher tower mode of the rotor-spar combination excited by the 4P frequency of 0.35 *Hz*.

5. Conclusion and outlook

This paper performs a code-to-code comparison between HAWC2 and SIMO-RIFLEX-AC for modelling the aerodynamics, hydrodynamics and structural dynamics of a VAWT mounted on a spar floater. Load cases in both steady and unsteady environments are designed to separately study the effect of dynamic stall, implementation of the AC flow theory and the fully coupled aero-hydro-servo-elastic capabilities.

The effect of dynamic stall is studied using the Stig Øye model and becomes significant at tip-speed ratios below 2.5. Here flow separation in the upwind rotor half reduces lift force, and consequently the downwind rotor half experiences increases inflow velocities. The numerical tools' solution to the AC flow problem contains a different induced velocity correction and inclusion of tangential terms, this has lead SIMO-RIFLEX-AC to calculate larger aerodynamic torque at wind speeds where $C_T \geq 0.50$. Fully coupled analyses with the spar VAWT brought forward that HAWC2's non-physical mooring system causes larger platform offsets, stronger surge-heave coupling and a natural frequency shift in both heave and yaw. The pitch response and fore-aft tower base bending moments in HAWC2 experience larger contributions from hydrodynamic loading, whereas mooring line tension is lower due to the absence of self-weight and wave loads. Regarding the flexible spar VAWT rotor, the first blade lead-lag mode is excited close to the 4P frequency. HAWC2 also shows a significant contribution at this frequency content in the fore-aft tower bending moments.

For future work it would be interesting to investigate the implication of the simplified nonlinear spring mooring model in HAWC2. Free decay tests could reveal differences about natural frequencies, whilst hydrodynamic loading analyses detail about the absence of wave loading on the mooring lines. Additionally, further understanding of the 0.34 *Hz* tower base response in HAWC2 can be gained by modal analysis of the rotor-spar combination.

Acknowledgements

The authors would like to appreciate the support from the Department of Marine Technology, Centre for Ships and Ocean Structures (CeSOS) and Centre for Autonomous Marine Operations and Systems (AMOS), Norwegian University of Science and Technology (NTNU), Trondheim, Norway. The second author would also like to appreciate the support from State Key Laboratory of Hydraulic Engineering Simulation and Safety (HESS-1710), Tianjin University, China.

References

[1] Paraschivoiu, I., 2002. Wind turbine design: with emphasis on Darrieus concept. Presses inter Polytechnique.
[2] Vita, L., 2011. Offshore floating vertical axis wind turbines with rotating platform. Technical University of Denmark, Lyngby, Denmark.
[3] Larsen, T.J. and Aagaard Madsen, H., 2013. On the way to reliable load simulation on VAWT's. Proceedings of EWEA 2013, Vienna.
[4] Cheng, Z., Madsen, H.A., Gao, Z. and Moan, T., 2017. A fully coupled method for numerical modeling and dynamic analysis of floating vertical axis wind turbines. Renewable Energy, 107, 604-619.
[5] Madsen, H. A., 1982. The Actuator Cylinder - A Flow Model for Vertical Axis Wind Turbines. The Institute of Industrial Constructions and Energy Technology, Aalborg, Denmark.
[6] Madsen, H. A., Larsen, T. J., Paulsen, U. S. and Vita, L., 2013. Implementation of the Actuator Cylinder Flow Model in the HAWC2 code for Aeroelastic Simulations on Vertical Axis Wind Turbines, in 51st AIAA Aerospace Sciences Meeting including the New Horizons Forum and Aerospace Exposition, Grapevine, Texas.
[7] Cheng, Z., Madsen, H.A., Gao, Z. and Moan, T., 2016. Aerodynamic modeling of floating vertical axis wind turbines using the actuator cylinder flow method. Energy Procedia, 94, 531-543.
[8] Øye, S., 1991. Dynamic stall, simulated as a time lag of separation. In Proceedings of the 4th IEA Symposium on the Aerodynamics of Wind Turbines, Harwell, UK.
[9] Bachynski, E.E., Kvittem, M.I., Luan, C. and Moan, T., 2014. Wind-wave misalignment effects on floating wind turbines: motions and tower load effects. Journal of Offshore Mechanics and Arctic Engineering, 136(4), p.041902.
[10] Cheng, Z., 2016. Integrated dynamic analysis of floating vertical axis wind turbines. PhD thesis, Norwegian University of Science and Technology, Trondheim, Norway.
[11] Cheng, Z., Wang, K., Gao, Z. and Moan, T., 2017. A comparative study on dynamic responses of spar-type floating horizontal and vertical axis wind turbines. Wind Energy 20(2), 305-323.
[12] Wang, K., Moan, T. and Hansen, M.O.L., 2013. A Method for Modeling of Floating Vertical Axis Wind Turbine. In Proceedings of the 32th International Conference on Ocean, Offshore and Arctic Engineering, Nantes, France.
[13] Johannessen, K., T.S. Meling, and S. Haver, 2002. Joint distribution for wind and waves in the northern North Sea. International Journal of Offshore and Polar Engineering, 12(1).